Image Anal Stereol 2026;45:141-152 doi: 10.5566/ias.3993
Original Research Paper

A ROBUST MORPHOLOGICAL APPROACH FOR AUTOMATED SEGMENTATION AND QUANTIFICATION OF SCRATCH ASSAY MICROGRAPHS

AYKUT ERDAMAR✉ AND TANSEL UYAR

Biomedical Engineering Department, Başkent University, Ankara, Turkey
e-mail: aerdamar@baskent.edu.tr, tuyar@baskent.edu.tr
(Received April 22, 2026; revised June 29, 2026; accepted June 30, 2026)

ABSTRACT

A variety of methodologies are available for the study of cell migration in vitro which has major function in physiological and pathophysiological processes even in cancer metastasis. The in vitro scratch assay is widely utilized for cell migration analysis. The straightforward, simple, and inexpensive procedure is performed manually; demonstrated to exhibit a high degree of similarity to the in vivo migratory behavior of cells. The scratch area is approximated to a rectangle or averaged to a certain number of parallel distances, performed by the analyst. Being laborious and time-consuming, the visual evaluation process is contingent upon the researcher's professional expertise, leading to subjective outcomes in the results. Furthermore, factors such as differing experimental setups, imaging equipment and brightness differences in the images can also lead to subjective outcomes. In order to circumvent inherent subjectivity, utilization of fully automatic software is proposed for the segmentation and quantification of scratch assay micrographs. The proposed software's algorithm is founded upon the principles of morphological image processing and rank filtering, encompassing a series of image processing steps. The results demonstrate that the software generates reproducible outputs even though parameters of the image such as brightness and contrast change. The algorithm offers a novel perspective in this field and functions as a robust and user-friendly computational instrument for end users, thereby reducing the subjectivity of the results.

Keywords: Cell migration, Image analysis, Imaging techniques, Scratch assay, Wound healing.

INTRODUCTION

Cell migration is the key step of many physiological and pathophysiological processes such as development, inflammation, tissue repair/regeneration, and cancer metastasis. There are different methods of studying cell migration in vitro. In vitro scratch assay, also known as the wound healing assay or wound healing (WH), was first introduced by Lampugnani (1999). The assay is widely used for the analysis of in vitro migration of cultured cells since it is a straightforward, easy, and inexpensive method (Song *et al.*, 2017; Somadder *et al.*, 2024; Soykan and Gunes, 2024; Yu *et al.*, 2024a;b; Kim *et al.*, 2025). In addition, it has a good mimicry of the in vivo migration behavior of cells and is compatible with real-time cell imaging (Liang *et al.*, 2007). It can also be adapted to a high-throughput screening platform (Yarrow *et al.*, 2004).

Scratch assay is based on the "healing" of a gap, or a scratch, created by scratching the fully confluent cell monolayer with a pipette tip. Due to the increment of soluble factors in the medium, cells polarize and protrude toward the scratch, contract and adhere to the surrounding matrix, and finally, they migrate to close the scratch (Small, 2013). Healing of the scratch is monitored over a time course by microscopy, scratch images are captured, and WH is evaluated according to variable parameters to determine cell migration via image analysis. The main limitation of the assay is the standardization of the assessment in terms of the techniques used and the end-point parameters selected. This is a general issue in all biological assays.

Scratch size and migration rate are two parameters for the quantification of cell migration. In manual analysis, the scratch size is measured in two ways. Firstly, the distance between two parallel lines at the boundaries of the scratch can be recorded. Secondly, the scratch area can be measured by tracing the sound boundaries (Topman *et al.*, 2012). There are different parameters for the determination of the migration rate. For example, the distance between the scratch edges is measured by at least ten random parallel horizontal points, and the mean values are calculated. The migration rate is expressed as a percentage of WH, calculated by dividing the scratch difference by the original scratch (Işeri *et al.*, 2014; Luan *et al.*, 2017).

Image analysis tools are frequently used for manual extraction of quantitative information (cell area, scratch size, scratch area, etc.). Visual analysis and

manual quantification of scratch assay images mainly depend on personal expertise, are time-consuming, and difficult. It may also have subjective consequences due to inter-experimentalist variability and experience. The challenge is to significantly accelerate with automated quantitative high-throughput image tools which enable acquiring objective and reproducible results. This case sparks great interest in the community of people using scratch assay.

To overcome these limitations, we have developed fully automatic software for the segmentation and quantification of scratch assay micrographs. The algorithm of this software is based on morphological image processing and rank filtering with several image processing steps. The goal of the study is to fulfill robustness and accuracy, concerning different experimental setups and/or image properties. Image parameters may vary due to different experimental setups and imaging equipment. Therefore, the software was designed to operate in the same way for all situations; and hence has flexibility for modification.

This study is an improved and expanded version of our previously presented work (Erdamar *et al.*, 2017). The main enhancements are the application of rank-filtering to detect scratch area substituting multi-thresholding in the previous work, and an extended image set for robustness. The rest of this article is organized as follows. Section 2 includes reviewing the related work. Section 3 begins with the description of the cell experimental setup and properties of the micrographs. Then, our approach to segmenting scratch areas is introduced. Appropriate ways to formulate this problem are described for each step. The results of the algorithm are given in Section 4. In Section 5, discussion of the results with previous studies and the proposed solutions by our method are considered. Finally, Section 6 constitutes the conclusion.

RELATED WORK

In the literature, there are limited studies about automated quantification of scratch assay images. The common goal of these studies is to get over the obstacles related to the image acquisition process and to elaborate specific design for the problem. The initial attempt was to develop a software tool based on the fast discrete curvelet transform for the automated analysis of monolayer scratch assays. Gebäck *et al.* (2009) confirmed the robustness of this algorithm on a diverse range of cell morphologies, under conditions of pharmacological stimulation or inhibition of migration and also in genetically manipulated cell lines. Topman *et al.* (2013) presented an automated and quantitative methodology for determining time-dependent damage areas in monolayer culture experiments. The utility of the method was represented by conducting scratch assay experiments in eight cultures of NIH3T3 fibroblast cells. Zaritsky *et al.* (2011) presented a segmentation algorithm to separate between multi-cellular and background regions for bright field images, based on a classification of local patches within an image, leading to evaluation of the scratch assay. Zordan *et al.* (2011) developed an automated image analysis algorithm based on texture segmentation capable of rapidly distinguishing between areas of the image covered by cells and the bare scratch area. Milde *et al.* (2012) introduced an algorithm and software for the automated analysis of cell migration in scratch assay under varying substrate conditions. Cortesi *et al.* (2017) developed a computational tool that computes the local entropy of micrographs to identify the scratch area. Glaß *et al.* (2012) proposed an automated method using the support vector machine. Three features were calculated from micrographs and the classification method defined cell boundaries. Vargas *et al.* (2016) presented a quantitative method for scratch assay analysis. This algorithm includes morphological and spatial filters and is based on the least squares method to fit curves for cell lines. Garcia-Fossa *et al.* (2020) presented PyScratch, a Python program for quantitative analysis of in vitro scratch assays. This software analyzed confluent cells and showed impact of high plating density affecting cell migration. Suarez-Arnedo *et al.* (2020) developed an optimized plugin for ImageJ, which automates the recognition of scratch size, corrects the average scratch width, and quantifies other parameters.

MATERIALS AND METHODS

MICROGRAPHS AND IMAGE ANALYSIS ALGORITHM

The experimental work was conducted at the Department of Molecular Biology and Genetics, Faculty of Arts and Sciences, Başkent University. The dataset under consideration comprises micrographs of human breast adenocarcinoma (MCF-7, ŞAP Institute, Ankara, Turkey) and human hepatocellular carcinoma (HepG2, ATCC, Rockville, MD, USA) cells. The cells were seeded in six-well plates at a density of 1×10^6 cells per well. Linear scratches were created on confluent cell monolayers using a pipette tip. The scratch areas were visualized using an inverted microscope (Olympus CK40) and captured with a digital camera (Eclipse E600, Nikon, Japan).

Micrographs were recorded at 24-hour intervals over a 72-hour time course. The raw RGB images were saved in JPEG format with a resolution of 2560×1920 pixels. The proposed image analysis algorithm, depicted in Fig. 1, was developed utilizing MATLAB (MathWorks, Inc.) and consists of three primary stages. The following subsections provide a detailed exposition of each stage of the algorithm.

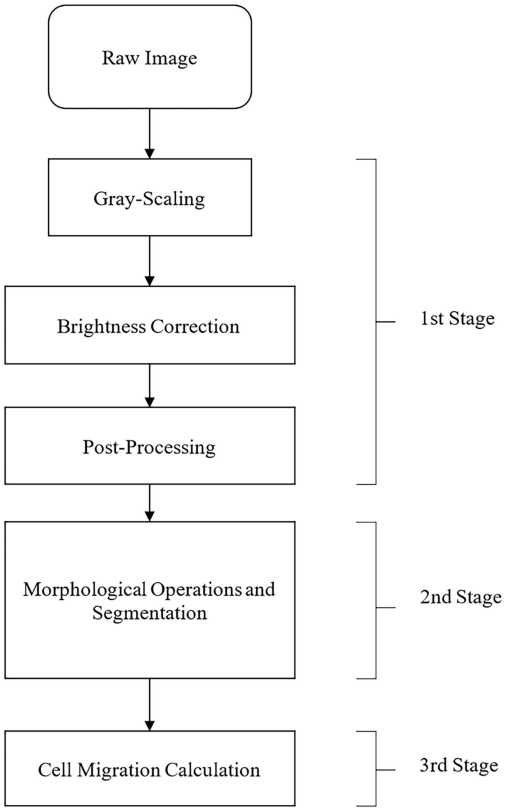

Fig. 1. *The flow chart of the scratch assay image analysis algorithm.*

IMAGE PROCESSING (1ST STAGE)

In the first step, the RGB image was converted into a grayscale image by using NTSC converting algorithm (Gonzalez and Woods, 2008). After the gray-scaling process, rank filtering was applied. Rank (order statistic) filters are non-linear spatial filters which are based on ordering (ranking) the values of a pixel contained in image area encompassed by the filter. The sample values $(X_1, X_2, \ldots, X_n)$ are lined up in ascending order using the rank filtering. The lined-up values were denoted by $X_{(1)}, X_{(2)}, \ldots, X_{(n)}$ and satisfy $X_{(1)} \leq X_{(2)} \leq \cdots \leq X_{(n)}$. The ranking process determines the response of the filter. Maximum rank filter in this study was used. This process replaced the value of a pixel with the maximum of the pixel value in its neighborhood (Heygster, 1982). Neighborhood window size was set as 25×25 pixels due to experimental trials. Maximum filtering was achieved using Eq. 1 and then applied to the grayscale image. Maximum rank filtering facilitates enhancing bright areas corresponding to cell locations in this study. Scratch areas remained nearly the same value. Rank filtered image (RFI) was obtained after the filtering process:

$$f(x,y) = \max_{(s,t)\in S_{xy}} \{g(s,t)\}. \tag{1}$$

where $f(x,y)$ is the intensity value of the pixel at coordinates (x,y), and S_{xy} denotes the 25×25 square neighborhood window centered at (x,y). The set of coordinates within this local window is formally defined as:

$$S_{xy} = \{(s,t) \in \mathbb{Z}^2 \mid x-12 \leq s \leq x+12, \; y-12 \leq t \leq y+12\}. \tag{2}$$

In the brightness correction process, scratch (inner) and cell (outer) areas were obtained through a segmentation process and a series of mathematical operations. In Fig. 2, these areas are marked on an exemplary scratch assay image. As a first step of the process sequence, the grayscale image was subtracted from the RFI, and a difference image was obtained. In the following step, the difference image was segmented with Otsu's segmentation (Otsu, 1979). Otsu's segmentation was applied to determine the cells surrounding the interior area. In this method, the image is assumed to be formed from two different pixel classes which are foreground and background pixels (Otsu, 1979). In this context, foreground pixels were cells and background pixels were scratch area. To obtain the scratch area, the outer area was subtracted from the grayscale image. Then, noise removal and sharpening processes were applied both for scratch and cell areas. Brightness correction steps are summarized in Fig. 2.

In the post-processing part, noise removal and sharpening, with an unsharp mask, were applied respectively. For the noise removal step, Wiener adaptive noise-removal filtering was used; it was preferred because it reduces the minimum mean squared error between the images, both at input and output (Lee, 1980; 1983). This process is aimed at reducing algorithm errors due to image noise. Intensity levels converged due to minimizing variance in locations where quantitative changes are low. For the first step, an $N \times M$ sized window was used for determining the local mean (Eq. 3) and variance around each pixel (Eq. 4). Next, a noiseless image b was obtained from the input image a by using local

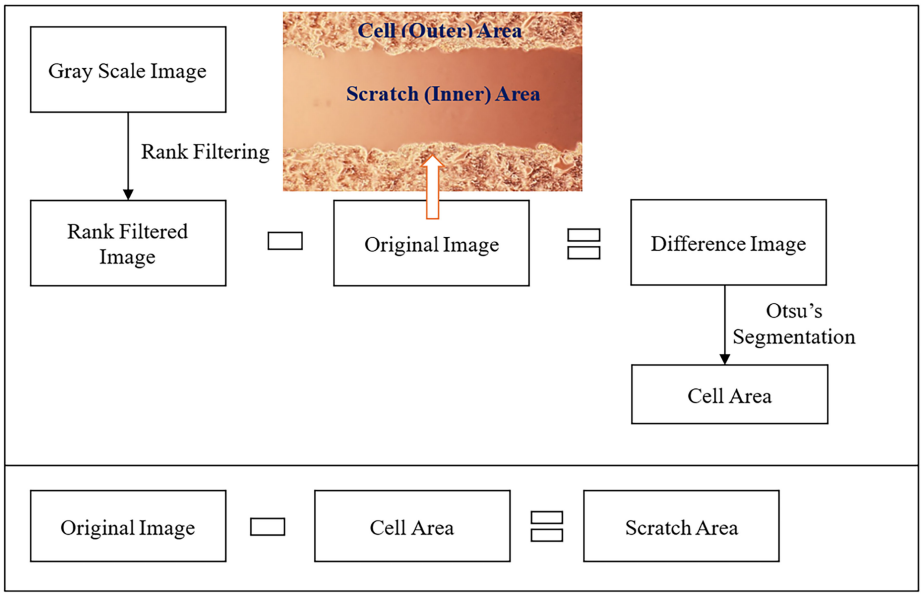

Fig. 2. *The flowchart, which illustrates a sample of a micrograph scratch assay image, delineates the process of brightness correction and the calculation of cell/scratch areas.*

mean μ, the variance around each pixel σ^2 and noise variance v^2 with Eq. 5 as follows:

$$\mu = \frac{1}{NM} \sum_{n_1,n_2 \in \eta} a(n_1,n_2) \tag{3}$$

$$\sigma^2 = \frac{1}{NM} \sum_{n_1,n_2 \in \eta} a^2(n_1,n_2) - \mu^2 \tag{4}$$

$$b(n_1,n_2) = \mu + \frac{\sigma^2 - v^2}{\sigma^2} (a(n_1,n_2) - \mu) \tag{5}$$

where n_1 and n_2 are indices of an image.

After the noise removal process, images h_o were sharpened with the unsharp masking method. According to Eq. 6, 5×5 sized and $\sigma = 1$ standard deviated Gaussian matrix h_g was constituted. The blurred new image h_b was obtained after the image had been processed with a Gaussian matrix in Eq. 7. The blurred image was subtracted from the original image, and the unsharp mask was created (Eq. 8). After subtraction, the original image and unsharp mask were summed to obtain the sharpened image h_s.

$$h_g(n_1,n_2) = e^{-\frac{n_1^2+n_2^2}{2\sigma^2}} \tag{6}$$

$$h_b(n_1,n_2) = \frac{h_g(n_1,n_2)}{\sum_{n_1} \sum_{n_2} h_g} \tag{7}$$

$$h_u(n_1,n_2) = h_o(n_1,n_2) - h_b(n_1,n_2) \tag{8}$$

$$h_s(n_1,n_2) = h_o(n_1,n_2) + h_u(n_1,n_2) \tag{9}$$

After obtaining the noise-free sharpened image, the morphological operations were initiated.

MORPHOLOGICAL OPERATIONS AND SEGMENTATION (2ND STAGE)

Morphological image processing is an approach for extracting desired image components. The image is used to probe some predefined shapes (i.e., structural elements) and to monitor how these elements influence the image. There are four basic operations of morphological image processing, namely dilation, erosion, opening, and closing (Gonzalez and Woods, 2008). The dilation operator grows or thickens objects in the image. Also, the dilation process is basically used to fill the holes in a continuous object. The erosion operator shrinks or thins objects in the image. Hence, it can be used to remove the noisy 'connection' between two objects (Srisha and Khan, 2013). The dilation and the erosion operations are defined in the order as follows:

$$X \oplus B = \{z \mid (\widehat{B})_z \cap X \neq \varnothing\} \tag{10}$$

$$X \ominus B = \{z \mid (B)_z \subseteq X\} \tag{11}$$

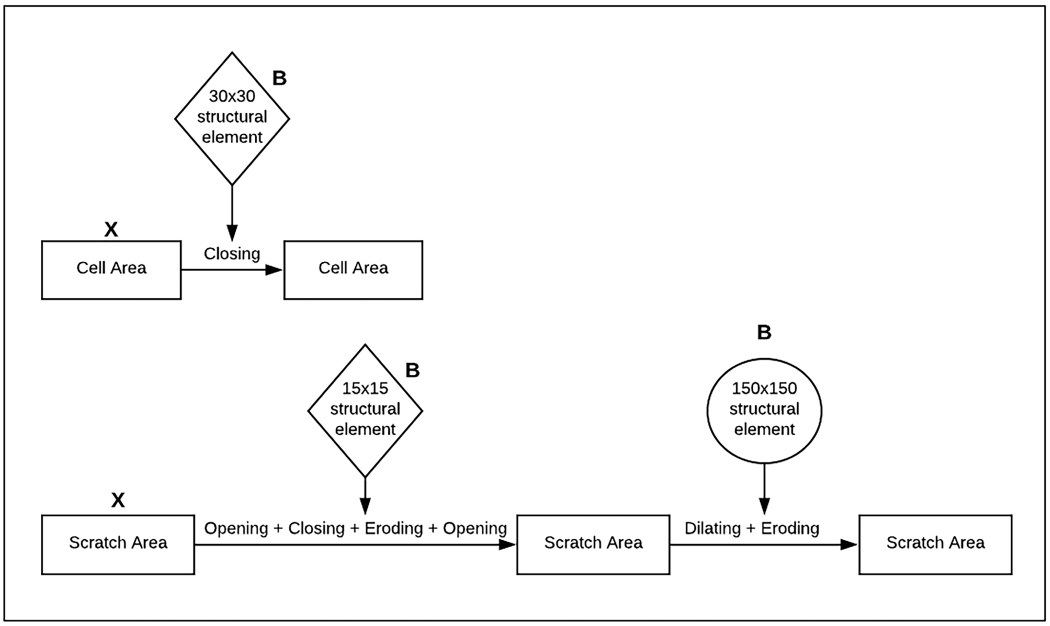

Fig. 3. *Flowchart detailing the specific sequence of morphological operations applied during Stage 2. The process maps two distinct pathways: the refinement of the cell area using a* 30×30 *pixel diamond-shaped structuring element (B), and the sequential refinement of the scratch area using a* 15×15 *diamond element followed by a* 150×150 *disk-shaped element.*

where X is an image, B is a structural element.

The opening and closing processes are a combinational operation of erosion and dilation (Srisha and Khan, 2013). The opening operator (Eq. 12) can be used to smooth the contour of an object, remove scrawny connections, and dissipate thin protrusions. The closing operator (Eq. 13) can be used to smooth the contour sections, remove small holes and fill gaps in the contour (Gonzalez and Woods, 2008).

$$X \circ B = (X \ominus B) \oplus B \tag{12}$$

$$X \bullet B = (X \oplus B) \ominus B \tag{13}$$

In this stage, a series of morphological operations were applied to obtain segmented scratch and cell areas. The initial operation was applied to the cell area. 30×30 pixel size 'diamond' type structural element was created. Afterward, the closing operation was applied using this structural element to obtain the final cell area. Following the above procedure, several morphological processes were applied to the scratch area. 15×15 pixel size 'diamond' type and 150×150 pixel size 'disk' type structural elements were created. Opening, closing, eroding and opening operations were applied in order by using the diamond-type element. Afterward, dilating and eroding operations were applied respectively by using the disk-type element. The complete step-by-step sequence of these morphological operations and their combination process is visually summarized in the flowchart (Fig. 3).

The separately obtained images, from morphological processes, were binary. The scratch and cell areas are both represented by "1" in these images. To make unification as a single image, each image was converted to an 8-bit gray level. To merge the scratch and cell areas, 255 gray level values were assigned to the scratch area, and 180 gray level values were assigned to the cell area, respectively. These values are defined according to experimental work to create an appropriate contrast in the image.

In Stage 2, a specific sequence of morphological operations was applied to binary images to refine the boundaries and extract the precise scratch and cell areas. As a final step, a set of morphological operations for hole-filling was executed to eliminate isolated background pixels within the cellular regions, ultimately yielding a solid and continuous binary mask for accurate quantification. Initially, a controlled dilation operation was employed for the iterative procedure (Eq. 14). When $k = 0$, the dilation process begins with a starting pixel chosen within the area of the complement of A. According to Eq. 14, the initial fragment X_{k-1} was dilated with a structural element

B and intersected with the complement of the original image (A'). The algorithm stops at the kth iteration when $X_k = X_{k-1}$. X_k is the final output of this process, and it was combined with image A according to Eq. 15. In this algorithm, a square-shaped structuring element B with a size of 3×3 (9 pixels) was specifically chosen to ensure isotropic expansion.

$$X_k = (X_{k-1} \oplus B) \cap A'; \qquad k = 1,2,3,\ldots \tag{14}$$

$$A_{filled} = A \cup X_k \tag{15}$$

CELL MIGRATION CALCULATION (3RD STAGE)

In the third stage, to determine the migration rate in the scratch assay, the area percentages were calculated by counting the pixels of the scratch area. The percentage of WH was calculated as follows (Işeri *et al.*, 2014):

$$WH\ (\%) = \left[\frac{A_{original\ scratch} - A_{healing}}{A_{original\ scratch}}\right] \times 100 \tag{16}$$

where $A_{original\ scratch}$ represents the area of the original scratch at $t = 0$, and $A_{healing}$ represents the area of the scratch at $t = 24$, 48, or 72 hours. Alternatively, the percentage of cell migration was expressed as follows:

$$Cell\ migration\ (\%) = \left[\frac{A_{cells} - A_{initial\ cells}}{A_{initial\ cells}}\right] \times 100. \tag{17}$$

where $A_{initial\ cells}$ represent an area of the cells in the scratch at $t = 0$, and A_{cells} represent an area of the cells in the scratch at $t = 24$h, 48h, or 72 hours.

RESULTS

OUTCOMES OF THE ALGORITHM

In the first stage of the algorithm, the RGB image is converted to grayscale. As seen in Fig. 4, brightness differences have occurred due to the illumination irregularity of the light source. In order to see these brightness irregularities more clearly, images were re-visualized as a jet colormap array and incorporated into Fig. 4. Rank filtering was applied to the grayscale image to obtain the scratch (inner) and cell (outer) areas. Maximum rank filtering was selected for enhancing cell areas in terms of pixel values. Upon examination of the jet colormap images, it was observed that the pixel values of the cells increased at each point following maximum rank filtering. However, scratch areas were not affected. Therefore, there were almost no changes in the pixel values of these areas. To correct the brightness difference, the grayscale image was subtracted from the RFI. After the process, the brightness difference in the image disappeared. Afterwards, binary images were obtained using Otsu's segmentation. Then, the scratch area was defined by subtracting the cell area from the grayscale image. Finally, post-processing operations were applied to the cell and scratch area images. The results of these processes are summarized in Fig. 4.

After the image brightness correction process, post-processing steps and a series of morphological operations were applied to obtain the final scratch and cell areas. Cell and scratch areas were summed, and morphological operations (filling holes) were finalized (Fig. 5). As the final step of the algorithm, the cell boundary was determined as a percentage of WH, and the cell migration was calculated.

COMPARISON OF MANUAL AND AUTOMATIC ANALYSIS

In order to evaluate the effectiveness and generalizability of the proposed algorithm, a diverse validation dataset consisting of a total of 32 scratch assay images was utilized. The dataset encompasses 16 image series from the MCF-7 cell line and 16 image series from the HepG2 cell line. To capture the full dynamic range of cell migration, images were acquired at 24-hour intervals over a 72-hour time course (0h, 24h, 48h, and 72h), presenting common experimental challenges such as uneven illumination, debris, and varying cell densities. To establish a robust baseline for comparison, four distinct sets of MCF-7 images – representing the most challenging visual conditions – were manually analyzed by three independent analysts. Subsequently, a comparative analysis was conducted between the automated boundaries determined by the algorithm and manual measurements.

The quantitative comparison between the manual and automatic approaches is presented in Fig. 6. In order to provide a clear illustration of the differences, the manual evaluations are represented by the mean of the three analysts, with error bars indicating the standard deviation. The findings indicate that the visual evaluation process is inherently vulnerable to subjectivity. Specifically, while there was a consensus

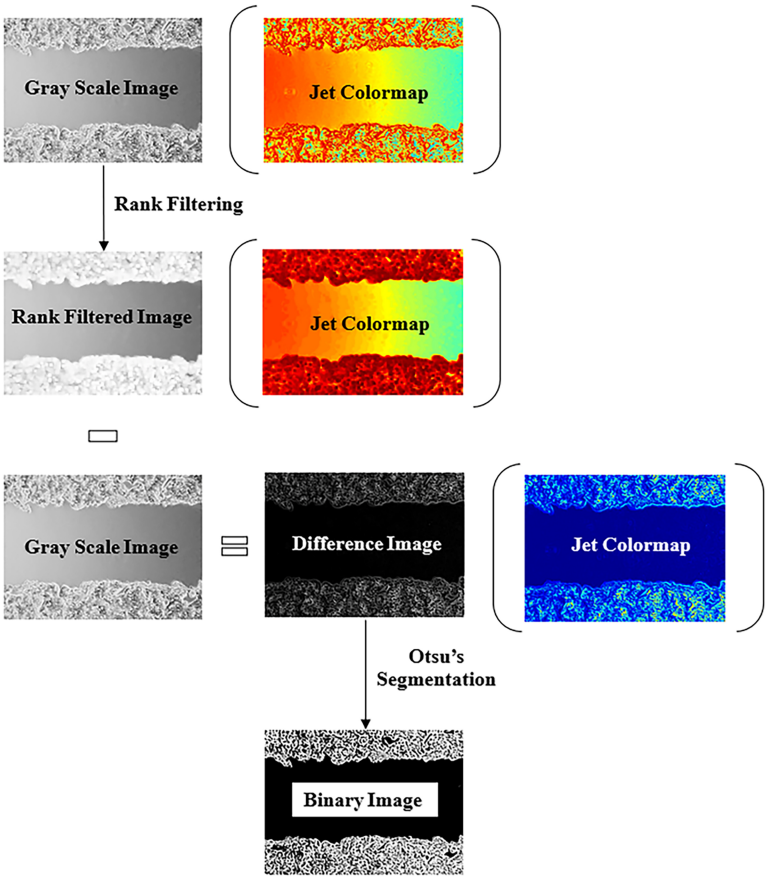

Fig. 4. *Brightness correction process in scratch assay images.*

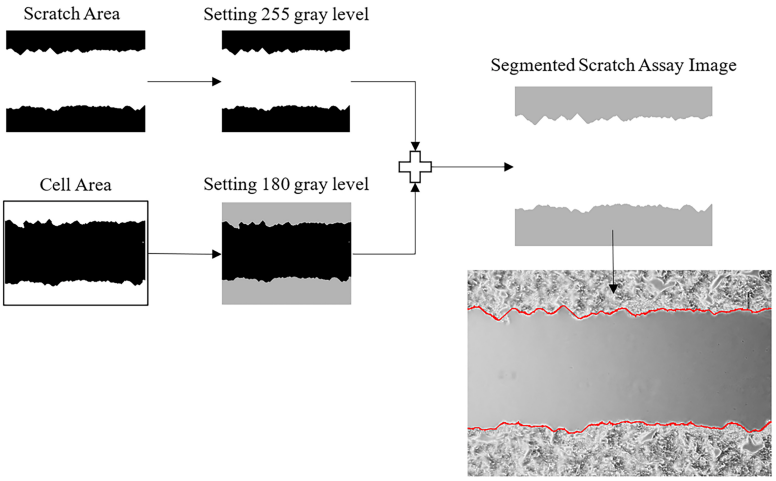

Fig. 5. *Figure depicting post-processing and morphological operations with segmented image boundaries.*

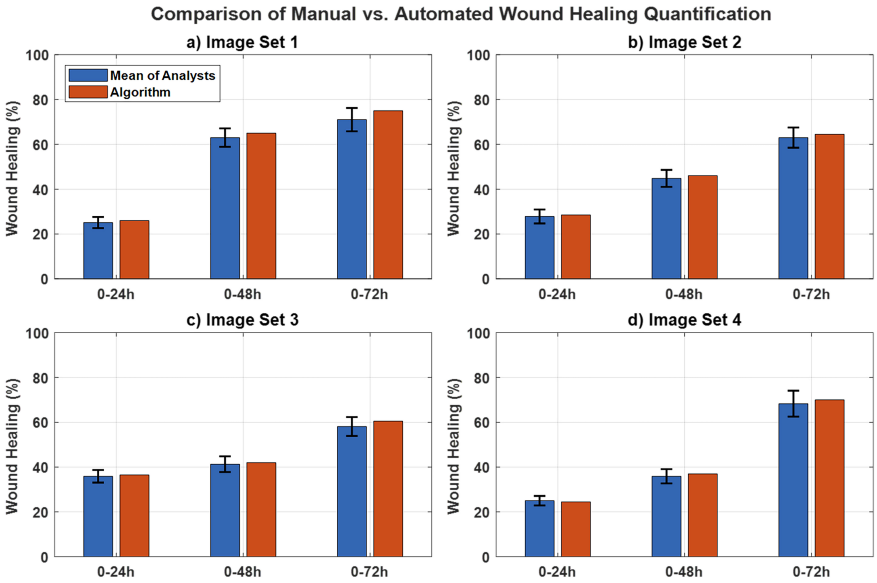

Fig. 6. *Comparison of manual evaluations (by three independent analysts) and the proposed automated algorithm for wound healing quantification across four different image sets (a–d) obtained from an MCF-7 cell line. The grouped bar charts present the mean percentage of wound healing determined manually versus the exact value calculated automatically for different time intervals (0–24 h, 0–48 h, and 0–72 h). The error bars on the manual evaluation columns represent the standard deviation among the three analysts, quantitatively highlighting the inherent subjectivity and inter-observer variability. This variability becomes more pronounced in later stages (e.g., 48h and 72h).*

among the analysts with low inter-observer variability during the initial stages of the assay (standard deviation of approximately 1.25% at 0–24h), this variability significantly increased at later time points, reaching up to 10.55% (48–72h). As the scratch boundaries became more irregular in these challenging later stages, the subjective manual measurements diverged. In contrast, the proposed algorithm provided a consistent, deterministic, and objective evaluation.

This discrepancy can be attributed to the fundamental differences between visual perception and computational morphology. In conditions that present significant visual challenges, such as instances of uneven lighting or sparsely distributed migrating cells, the human eye has a tendency to approximate the gap boundaries, frequently smoothing over the true, irregular micro-extensions of the cell front. In contrast, the algorithm performs an objective evaluation based on local pixel intensities, independent of visual approximations. Consequently, the algorithm consistently captures the actual microscopic roughness and true boundaries of the migration area, ensuring reproducible and precise quantification that human observation cannot reliably match. As demonstrated in Fig. 7, the scratch boundaries defined by the algorithm are effectively delineated by red lines across all time intervals.

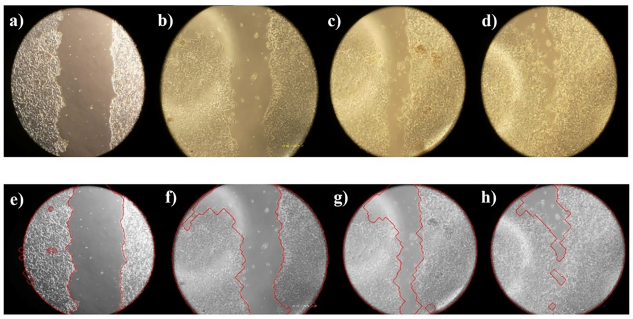

Fig. 7. *Representative scratch assay micrographs and their corresponding automated segmentations over a 72-hour time course. The top row displays the raw images captured at (a) 0h, (b) 24h, (c) 48h, and (d) 72h. The bottom row (e–h) shows the respective algorithm outputs, where red lines delineate the precise scratch boundaries (Image Set 1, MCF-7 cell line).*

COMPARISON WITH A CONVENTIONAL AUTOMATED TOOL

To validate the robustness and practical advantages of the proposed algorithm, a comparative analysis was performed using the widely used open-source “Wound Healing Size Tool” plugin in ImageJ/Fiji (Suarez-

Arnedo *et al.*, 2020). For this comparative analysis, the image set displayed in Fig. 7 (Image Set 1, MCF-7 cell line) was selected. The outputs of the ImageJ tool are presented in Fig. 8. The ImageJ tool demonstrated a high degree of parameter dependency and subjectivity. To achieve acceptable segmentation in the 0h, 24h, and 48h frames, it was necessary to manually adjust three different parameters (variance window radius, threshold value, and percentage of saturated pixels) for almost every image, through a process of trial and error. Furthermore, within the 72-hour frame, characterized by narrow and uneven lighting effects, the ImageJ plugin demonstrated an inability to detect the scratch boundaries, irrespective of parameter tuning. In contrast, the proposed algorithm successfully and automatically isolated the scratch area across all time frames, including those in extreme conditions at 72 hours, without requiring any image-by-image user intervention. This underscores the enhanced robustness of the proposed method against illumination artefacts and its capacity to eradicate user-induced subjectivity.

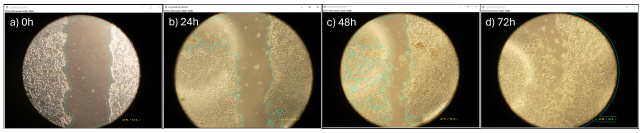

Fig. 8. *Segmentation results obtained using the ImageJ "Wound Healing Size Tool" on the same MCF-7 image series evaluated in Fig. 7. The panels display the best possible segmentation outcomes achieved after extensive manual parameter tuning for each specific frame at (a) 0h, (b) 24h, (c) 48h, and (d) 72h. While the tool managed to approximate boundaries in the early stages through continuous user intervention, it completely failed to detect the narrow scratch area under uneven lighting conditions at 72h (d), resulting in severe mis-segmentation.*

EXAMINING ANALYSIS TIME

Another fundamental aspect of scratch assays is the time required to perform the analysis. Depending on the size of the image data set, elaborative analysis of the images might be very time-consuming. Furthermore, repetitive actions may cause fatigue during manual analysis; leading to different results even in the analysis of the same image. In the manual analysis, the mean duration of the analysts was 560 ± 30 seconds for 16 images. On the other hand, the developed algorithm analyzed only 35.5 seconds for the same 16 images. According to this numerical data, the manual analysis duration of an image is equal to the automatic analysis duration of sixteen images. Therefore, the use of automated approaches creates significant differences and improvements in the analysis of very large data sets.

DISCUSSION

The manual method for scratch assay involves approximating the scratch area to a rectangle or averaging a certain number of parallel distances. The utilization of the manual method has been demonstrated to be a protracted process, with a considerable degree of reliance on the professional expertise of the analyst. The reliability and objectivity of this method are potentially compromised when analyzing a substantial number of images. The achievement of precise outcomes through manual techniques is contingent upon the parallel alignment of the scratch area. Moreover, analysts must maintain consistency when delineating rectangles and measuring parallel distances. At present, the quantification of the scratch assay is based on the manual analysis of the scratch area at different time intervals following the initial scratch.

The serious problem in this process is the necessity of fine adjustment of the image captured at two different time points. For example, as shown in Fig. 7, differences in the lighting or alignment of the photographic equipment in images taken at different times in the same scratch test can cause changes in brightness and contrast. These differences cannot be distinguished visually. The tools used in manual analysis lack the ability to determine these differences. The ImageJ macro is a widely utilized tool for scratch assay, with a relatively decreasing level of user dependency. Cortesi *et al.* (2017) expressed favorable results with automated methods, which produce less inaccurate but objective results in scratch area segmentation compared to manual methods.

However, comparative evaluations with the ImageJ/Fiji "Wound Healing Size Tool" demonstrated that conventional thresholding-based tools are highly susceptible to parameter dependency. In our tests, the ImageJ plugin required continuous manual optimization for different time frames (0h, 24h, 48h), leading to laborious and subjective outcomes. Furthermore, in challenging frames (e.g., 72h) where the scratch area was minimal and uneven lighting was present, the conventional tool failed to perform segmentation entirely. The proposed morphological approach, however, successfully and automatically segmented all time frames without requiring manual parameter tuning, proving its robustness against lighting artifacts.

The presented image processing method for automated analysis of the scratch assay does not require standardized objectives and/or special equipment. In addition, it is easy to apply to micrographs, as no manual intervention or pre-calibration is required. We analyzed images of two cell lines captured by different users at different time intervals using the proposed method. The morphology of MCF-7 cells and HepG2 cells was observed and revealed variable scratch edges. We also analyzed low-quality images with irregular edges of the scratches. Our method is robust and yields reproducible results. Manual intervention during analysis is eliminated, providing a significant advantage. Along this line, successful collaboration of multidisciplinary researchers is the key for application of new methodologies and creative innovations.

In the literature, almost every study uses its own images and manual analysis by the expert, and the verification criterion is assumed to be the gold standard. Therefore, it is not possible to make a one-to-one comparison of the results of this study with previous studies. Furthermore, other automated analysis methods described in the literature do not provide a suitable solution for different contrasts or brightness levels. While a method may perform well on an image with uniform illumination, it may not perform as well when the image set changes. We drew attention to this issue in our previous study (Erdamar *et al.*, 2017), and the presented method was developed to produce reproducible results in images with different contrast and illumination distributions. In our algorithm, each analysis is performed individually and independently of images captured at different time intervals. The robustness of the method may allow researchers to record the kinematic parameters of cultures at multiple time points. Consequently, the migratory behavior of cells over the entire period can be obtained with greater reliability. Overall, our results are in agreement with similar studies using individual approaches.

CONCLUSION

In this study, an automated, robust method was introduced for the quantification of cell migration rates in monolayer cultures exposed to locally induced damage using the scratch assay. The efficacy of the presented method has been compared with the manual technique and the ImageJ macro, and a significant improvement in image analysis has been demonstrated.

This algorithm makes it possible to analyze a large number of images with irregular brightness in a short time. The images were captured at different time intervals by different analysts: the actual experimental situation of most studies. In addition, edge irregularity problems, which depend mostly on morphological variations of cells, such as size and shape, were overcome by the algorithm. In fact, edge irregularity becomes more drastic as assay time prolongs without healing of the wound since some cells detach from the culture flask. We have analyzed these low-quality images and yielded reproducible results. Using this algorithm also gave reproducible results with different cell lines. In conclusion, image analysis of the scratch assay is experiment-dependent, time-consuming, and requires personal expertise, and may produce subjective results. Therefore, this algorithm not only provides a new insight into the area but also enables a user-friendly computational tool for the end users.

AVAILABILITY OF DATA AND MATERIAL

Access to the data is restricted due to an ongoing institutional research project. Metadata, all image sets, and MATLAB implementation scripts are privately available at `https://zenodo.org/records/19653335`. Qualified researchers may request access for validation purposes by contacting the corresponding author via institutional email. Data sharing requires a formal Data Transfer Agreement (DTA).

COMPETING INTERESTS

The authors declare no competing interests.

FUNDING

Not applicable.

AUTHORS' CONTRIBUTIONS

A.E. and T.U. conceived the idea; A.E. and T.U. analyzed the data; and T.U. led the writing; A.E. revised and edited the manuscript. All authors have read and approved the final version of the manuscript.

ACKNOWLEDGEMENTS

The Department of Molecular Biology and Genetics, Faculty of Arts and Science, Başkent University is gratefully acknowledged for the scratch assay images.

REFERENCES

Cortesi M, Pasini A, Tesei A, Giordano E (2017). Aim: A computational tool for the automatic quantification of scratch wound healing assays. Appl Sci 7:1237.

Erdamar A, Yilmaz S, Uyar T, Iseri O (2017). A new image segmentation method for quantitative analysis of in vitro scratch assay. In: 2017 25th Signal Processing and Communications Applications Conference (SIU). Antalya, Türkiye: IEEE.

Garcia-Fossa F, Gaal V, de Jesus M (2020). Pyscratch: An ease of use tool for analysis of scratch assays. Comput Methods Programs Biomed 193:105476.

Gebäck T, Schulz M, Koumoutsakos P, Detmar M (2009). Tscratch: A novel and simple software tool for automated analysis of monolayer wound healing assays. Biotechniques 46:265–74.

Glaß M, Möller B, Zirkel A, Wächter K, Hüttelmaier S, Posch S (2012). Cell migration analysis: Segmenting scratch assay images with level sets and support vector machines. Pattern Recognit 45:3154–65.

Gonzalez R, Woods R (2008). Digital Image Processing. Upper Saddle River, New Jersey, 3rd ed.

Heygster G (1982). Rank filters in digital image processing. Comput Graph Image Process 19:148–64.

Işeri Ö, Sahin F, Terzi Y, Yurtcu E, Erdem S, Sarialioglu F (2014). Beta-adrenoreceptor antagonists reduce cancer cell proliferation, invasion, and migration. Pharm Biol 52:1374–81.

Kim J, Choi H, Kim C, Chung T, Kim K (2025). Enhanced effect of the leaves extract from prunus persica var. nucipersica on antioxidation, collagen synthesis, re-epithelialization and angiogenesis for the improvement of skin wound healing. Biotech Histochem 100:279–90.

Lampugnani M (1999). Cell migration into a wounded area in vitro. Methods Mol Biol 96:177–82.

Lee J (1980). Digital image enhancement and noise filtering by use of local statistics. IEEE Trans Pattern Anal Mach Intell PAMI-2:165–8.

Lee J (1983). Refined filtering of image noise using local statistic. Comput Graph Image Process 24:255–69.

Liang C, Park A, Guan J (2007). In vitro scratch assay: a convenient and inexpensive method for analysis of cell migration in vitro. Nat Protoc 2:329–33.

Luan S, Hao R, Wei Y, Chen D, Fan B, Dong F, Guo W, Wang J, Chen J (2017). A microfabricated 96-well wound-healing assay. Cytometry A 91:1192–9.

Milde F, Franco D, Ferrari A, Kurtcuoglu V, Poulikakos D, Koumoutsakos P (2012). Cell image velocimetry (civ): Boosting the automated quantification of cell migration in wound healing assays. Integr Biol Camb 4:1437–47.

Otsu N (1979). A threshold selection method from gray-level histograms. IEEE Trans Syst Man Cybern 9:62–6.

Small J (2013). Cell migration. In: Lennarz W, Lane M, eds., Encyclopedia of Biological Chemistry. San Diego: Elsevier, 2nd ed., 430–5.

Somadder R, Faraj L, Datta S, Kanapathipillai M, Ghosh G (2024). Effect of extracellular matrices on production and potency of mesenchymal stem cell-derived exosomes. Biotechnol J 19:e2300474.

Song Z, Li S, Dong J, Sun M, Zhang X, Shu R (2017). Enamel matrix proteins regulate hypoxia-induced cellular biobehavior and osteogenic differentiation in human periodontal ligament cells. Biotech Histochem 92:606–18.

Soykan M, Gunes S (2024). Overexpression of klotho gene using crispr/cas9 induces apoptosis and inhibits cell motility in the human colorectal cancer cells. Biotechnol J 19:e2300496.

Srisha R, Khan A (2013). Morphological operations for image processing: Understanding and its applications. In: 2013 National Conference on VLSI, Signal processing & Communications. India.

Suarez-Arnedo A, Figueroa F, Clavijo C, Arbeláez P, Cruz J, Muñoz-Camargo C (2020). An image j plugin for the high throughput image analysis of in vitro scratch wound healing assays. PLoS One 15:e0232565.

Topman G, Lin F, Gefen A (2013). The natural medications for wound healing - curcumin, aloe-vera and ginger - do not induce a significant effect on the migration kinematics of cultured fibroblasts. J Biomech 46:170–4.

Topman G, Sharabani-Yosef O, Gefen A (2012). A standardized objective method for continuously measuring the kinematics of cultures covering a mechanically damaged site. Med Eng Phys 34:225–32.

Vargas A, Angeli M, Pastrello C, Mcquaid R, Li H, Jurisicova A, Jurisica I (2016). Robust quantitative scratch assay. Bioinformatics 32:1439–40.

Yarrow J, Perlman Z, Westwood N, Mitchison T (2004). A high-throughput cell migration assay using scratch wound healing, a comparison of

image-based readout methods. BMC Biotechnol 4:21.

Yu F, Chen Y, Yi W, Guan M, Lin N, Zhuo Y, Lin J, Lai F (2024a). Lung-specific exosomes for doxorubicin delivery in lung adenocarcinoma therapy. Biotechnol J 19:e2300296.

Yu J, Huang D, Liu H, Cai H (2024b). Optimizing conditions of polyethylene glycol precipitation for exosomes isolation from mscs culture media for regenerative treatment. Biotechnol J 19:e202400374.

Zaritsky A, Natan S, Horev J, Hecht I, Wolf L, Ben-Jacob E, Tsarfaty I (2011). Cell motility dynamics: A novel segmentation algorithm to quantify multicellular bright field microscopy images. PLoS One 6:e27593.

Zordan M, Mill C, Riese D, Leary J (2011). A high throughput, interactive imaging, bright-field wound healing assay. Cytometry Part A 79:227–32.